V International Conference on Particle-based Methods – Fundamentals and Applications
PARTICLES 2017
P. Wriggers, M. Bischoff, E. Oñate, D.R.J. Owen, & T. Zohdi (Eds)

NUMERICAL SIMULATION OF SOLIDIFICATION PHENOMENA OF MOLTEN DROPLET AT DIFFERENT IMPACT VELOCITY

S. KONDO[1], H. MAMORI[2], N. FUKUSHIMA[3], AND M. YAMAMOTO[2]

[1]Graduate School of Mechanical Engineering, Tokyo University of Science
6-3-1 Niijuku, Katsusika-ku, Tokyo, 125-8585, Japan
e-mail: 4516618@ed.tus.ac.jp

[2]Department of Mechanical Engineering, Tokyo University of Science
6-3-1 Niijuku, Katsusika-ku, Tokyo, 125-8585, Japan

[3]Department of Prime Mover Engineering, Tokai University
4-1-1 Kitakaname, Hiratsuka-shi, Kanagawa, 259-1292, Japan

Key words: Deposition phenomena, molten droplet, heat transfer, explicit-moving particle simulation

Abstract. Jet engines ingest sand and volcanic ash in the air and then the sand and ash reach a combustion chamber. Due to the high temperature of the chamber, sand and ash are melted and form the molten droplets. The molten droplets are rapidly cooled around the turbine blades and the end walls. The droplets are solidified and finally adhere on these surfaces. This deposition phenomenon causes many problems in the aircraft, e.g., deterioration of the turbine performance, disturbing the cooling flow of turbine blade, etc. To predict or prevent the deposition phenomenon, its mechanisms should be clarified. In the present study, we perform three-dimensional numerical simulations on deposition behavior of a single molten droplet on a cooled substrate. We compare the present numerical data and the experimental data in the previous study for validation and we observe effects of the drop velocity on the deposition phenomenon. As a numerical method, an explicit-moving particle simulation method is employed since the method is suitable for the large interface deformation system. The computational results show reasonable agreements with the experimental data, especially, at an early stage of the deposition. We confirm finger-like-structures which is a characteristic shape of the adhered droplet edge. As increasing of the initial droplet velocity, we found that the increase of the rebound particles.

1 INTRODUCTION

When jet engines are operated on volcanic ash clouds or sandy ground, sand or ash are ingested and melted in a high temperature combustion chamber. Because turbine components (e.g., blades, cooling flow orifices, end-walls, etc.) are colder than molten droplets, some droplets adhere and accrete on these surfaces. The deposition phenomenon does not only leads to deterioration of the turbine performance (e.g., blade performance and cooling effect [1]), but also increase the maintenance cost. Therefore, the prediction and understanding of the deposition phenomena are of importance from the engineering viewpoint. In previous studies,

for example, Webb et al. [2] made an experimental study for the coal ash deposition. They evaluated and quantified thickness sediments for four different ash types. They have shown that the chemical makeup of the ash also plays a crucial role in deposition formation and thickness. Although experiments in the research are conducted under some conditions, Computational Fluid Dynamics (CFD) makes it easier to apply various conditions.

Moreover, in the gas turbine, it is difficult to install some proves to measure the deposition phenomenon due to high temperature and pressure. Accordingly, we employ a numerical approach. As for a first step, in the present study, we focus on the deposition phenomenon of a single melted droplet on a flat surface. We can refer to a review about drop impact on a surface [3]. While engine components have a complex geometry and there are many melted droplets flowing in the gas turbine, the present simplified system (i.e., deposition of a single droplet on a flat surface) is expected to give us some physical insights of the deposition behavior.

The objectives of the present study are to simulate and investigate deposition behavior of a single melted droplet on a flat surface. Since a droplet has interfaces, which are largely deformed when it collides on the flat plate, we have employed an explicit moving particle method [4, 5] (referred to as the E-MPS method, hereafter). The E-MPS method is one of the Lagrangian methods. At first, we show comparisons between the present numerical results and the existing experimental data in the previous study [6] and discuss influences of the initial drop velocity on the deposition behavior.

2 CALCULATION METHOD

2.1 E-MPS METHOD

In the E-MPS method, the fluid motion is reproduced by computational particles. The fluid motion is governed by the continuity and Navier-Stokes equations, as

$$\frac{\partial \rho}{\partial t} = 0, \tag{1}$$

$$\frac{Du}{Dt} = -\frac{1}{\rho}\nabla P + \nu \nabla^2 u + g + \frac{1}{\rho}\sigma\kappa\delta n, \tag{2}$$

respectively. Here, u is velocity vector, ρ is density, P is pressure, ν is kinematic viscosity, g is acceleration of the gravity, σ is surface tension coefficient, κ is curvature, δ is the delta function, and n is the normal vector. For the spatial discretization of the governing equations, the following gradient and Laplacian models are employed as,

$$\nabla \phi = \frac{d}{n^0} \sum_{j \neq i} \frac{\phi_j - \phi_i}{\left|\mathbf{r}_{ij}\right|^2} \mathbf{r}_{ij} w_{ij}, \tag{3}$$

$$\nabla^2 \phi = \frac{2d}{\lambda n^0} \sum_{j \neq i} \left(\phi_j - \phi_i\right) w_{ij} . \tag{4}$$

Here, ϕ is physical quantity such as velocity, d is dimensional number of calculation, n^0 is the number of density of the particles, and w_{ij} is a weight function. The subscripts of i and j are indices of computational particles and $\mathbf{r}_{ij}$ is a distance vector between particles, indices of which are i and j. The coefficient λ is defined by Eq. (5).

$$\lambda = \frac{\sum_{j \neq i} \left| r_j - r_i \right|^2 w\left(\left| r_j - r_i \right| \right)}{\sum_{j \neq i} w\left(\left| r_j - r_i \right| \right)}, \tag{5}$$

where r_i is a coordinate vector of i th particle and w is a weight function for average. Since the droplet is solidified on a surface due to heat transfer, the energy equation, Eq. (6), is also solved in this simulation.

$$\frac{DT}{Dt} = \frac{k}{\rho C_P} \nabla^2 T + \frac{1}{\rho C_P} Q. \tag{6}$$

Here, T is temperature, C_p is specific heat, k is thermal conductivity, and Q is amount of heat generation. The Laplacian model (as shown in Eq. (4)) is also applied to Eq. (6) and the discretized energy equation is written by the following equation,

$$T_i^{n+1} = T_i^n + \frac{k_i}{\rho_i C p_i} \Delta t \frac{2d}{n\lambda} \sum_j (T_j^n - T_i^n), \tag{7}$$

when a target computational particle, index of which is i, is affected by surrounding either coagulated particles or melted particles, indices of which are j. Here, Δt is a size of time step and the superscript of n is time step. When a target computational particle, index of which is i, is affected by both surrounding coagulated particles and melted particles, indices of which are j, we apply the following discretized equations,

$$T_i^{n+1} = T_i^n + \frac{k_i}{\rho_i C_i} \Delta t \frac{2d}{n\lambda} \sum_j \frac{1}{2} (T_s^n - T_i^n), \tag{8}$$

$$T_s = \frac{\sqrt{\rho_i C_i k_i} T_i^n + \sqrt{\rho_j C_j k_j} T_j^n}{\sqrt{\rho_i C_i k_i} + \sqrt{\rho_j C_j k_j}}. \tag{9}$$

Here, T_s denotes the mean temperature between a target particle and a surrounding particle in the solid or liquid phase. The physical properties, ρ, C_p and k with the subscripts of i and j denotes the properties on i th and j th particles, respectively.

2.2 SOLIDIFICATION MODEL

The latent heat h_{ls} play an important role in a deposition phenomenon. Figure 1 explains our solidification model including the latent heat effects. The initial condition of a droplet is in a liquid phase. When the droplet temperature, T, reaches the melting temperature, $T_{melting}$, the liquid-computational particles are in a transient state with the constant temperature at $T_{melting}$. When the computational particles lose the latent heat, h_{ls}, the computational particles are treated as solid-phase particles. We define the liquid fraction, γ_m: γ_m=0 in a solid phase; $0<\gamma_m<1$ in a transient phase; $\gamma_m = 1$ in a liquid phase, as shown in Eq. (10).

$$\begin{array}{lll} Solid & when & \left(\quad T < T_{liquidus} \quad , \quad \gamma_m = 0 \quad \right) \\ Transient & when & \left(\quad T = T_{liquidus} \quad , \quad 0 < \gamma_m < 1 \quad \right) \\ Liquid & when & \left(\quad T > T_{liquidus} \quad , \quad \gamma_m = 1 \quad \right) \end{array} \tag{10}$$

$$\gamma_m^{n+1} = \gamma_m^n + \frac{\Delta h}{h_{ls}} \tag{11}$$

The time advancement of the liquid fraction, γ_m, is described in Eq. (11). Here, Δh denotes the enthalpy change between particles in a transient phase. Δh is calculated by the following heat conduction equation, Eq. (12) or Eq. (13)

$$\Delta h = \frac{\Delta t}{\rho_i} \frac{2d}{\lambda n_i} \sum_{j \neq i} \left\{ k_{ij} \left(T_j - T_i \right) w_{ij} \right\} \tag{12}$$

Equation (12) is applied when both particles i and j are not in the transient phase. The enthalpy change, Δh, between particles in different phases is computed by Eq. (13) using T_s defined in Eq. (9).

$$\Delta h = \frac{\Delta t}{\rho_i} \frac{2d}{\lambda n_i} \sum_{j \neq i} \frac{1}{2} \left\{ k_{ij} \left(T_s - T_i \right) w_{ij} \right\} \tag{13}$$

Mean thermal conductivity, k_{ij}, in Eqs. (12) and (13) is calculated from thermal conductivity of particles i and j in the following equations [7], Eq. (14) or Eq. (15).

$$k_{ij} = 2k_i k_j / \left(k_i + k_j \right) \tag{14}$$

$$k_{ij} = \begin{cases} k_j & when \quad \left(i : Transient \right) \\ k_i & when \quad \left(j : Transient \right) \end{cases} \tag{15}$$

When both particles i and j are not in the transient phase, we use Eq. (14) to calculate the mean thermal conductivity. Equation (15) indicates that, when particle i is in a transient phase, we use the thermal conductivity of particle j; when particle j is in a transient phase, we use the thermal conductivity of the particle i as k_{ij}.

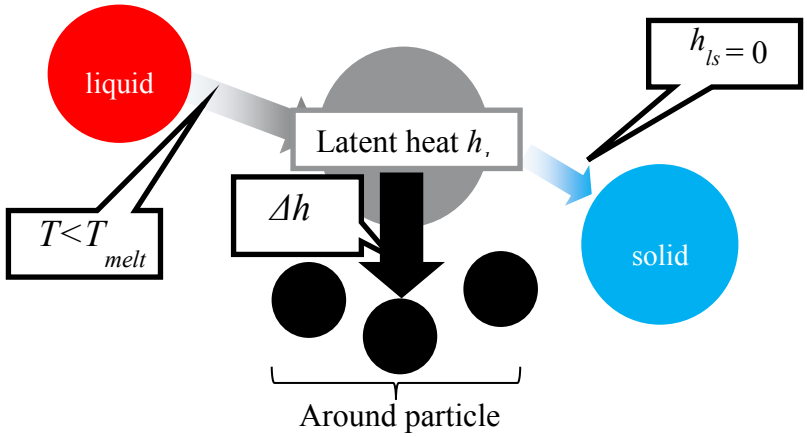

Figure 1 Schematics of a solidification model.

3 COMPUTATIONAL CONDITION

Figure 2 shows the initial condition of a droplet. A single molten droplet collides and adheres on a cooled flat plate. The numerical condition in the present study is set to be similar to the experiments conducted by Shakeri and Chandra [6]: the droplet consists of Sn; the collision angle of 90 degree; the initial diameter of the droplet D_0 is set to be 2.2 [mm]; the initial temperature of the droplet is 519 [K]; the substrate is made by stainless steel; the substrate temperature is kept constant at T_{wall} = 298 [K]. The simulations are conducted at three different collision velocities, v_0 = 10, 20 and 30 [m/s] to clarify effects of collision velocity. In addition, the simulation in the case of the collision velocity of 4.0 [m/s] is also performed to validate our simulation by comparison with the experimental data [6]. In Table 1, the physical properties of Sn are summarized. The droplet is represented by aggregation of computational particles. The number of computational particles is about 195,000. Initial state of all the computational particles is liquid. In the coagulation model, the latent heat is considered as described in section 2.2.

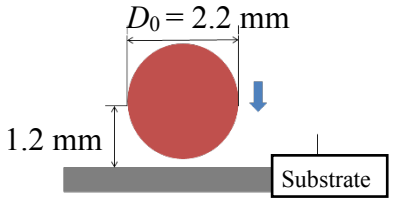

Figure 2 Initial condition of a single molten droplet.

Table 1 Physical properties of Sn.

Properties	Symbol		
Thermal conductivity	k_{liquid}	[W/mK]	33.6
	k_{solid}	[W/mK]	62.2
Specific heat	$C_{p\ liquid}$	[J/kgK]	244
	$C_{p\ solid}$	[J/kgK]	226
Density	ρ_{liquid}	[kg/m^3]	6,980
	ρ_{solid}	[kg/m^3]	7,200
Melting temperature of Sn	$T_{melting}$	[K]	505

4 RESULTS AND DISCUSSION

Figure 3 shows a time series of snapshots of a colliding and adhering molten Sn droplet when the collision angle is 90 degree. The time t begins when the droplet starts falling. The collision velocity is 4 m/s. The liquid, transient (i.e. liquid to solid), and solid particles are colored by red, white, and blue, respectively. We observed that the droplet collides, spreads, and coagulates on the surface of the substrate. The behavior reasonably agrees with the experimental results [6]. Furthermore, finger-like-structures, which are typical structures in the deposition, are observed at the circumference of the adhered droplet as shown in Fig. 3(l) (pointed out by the red circle).

Figure 4 shows a time series of snapshots of the droplet from the side view. We found the clearance between the edge of the droplet and the substrate. These characteristics are also observed in the experiment conducted by Tabbara et al. (2012) [8].

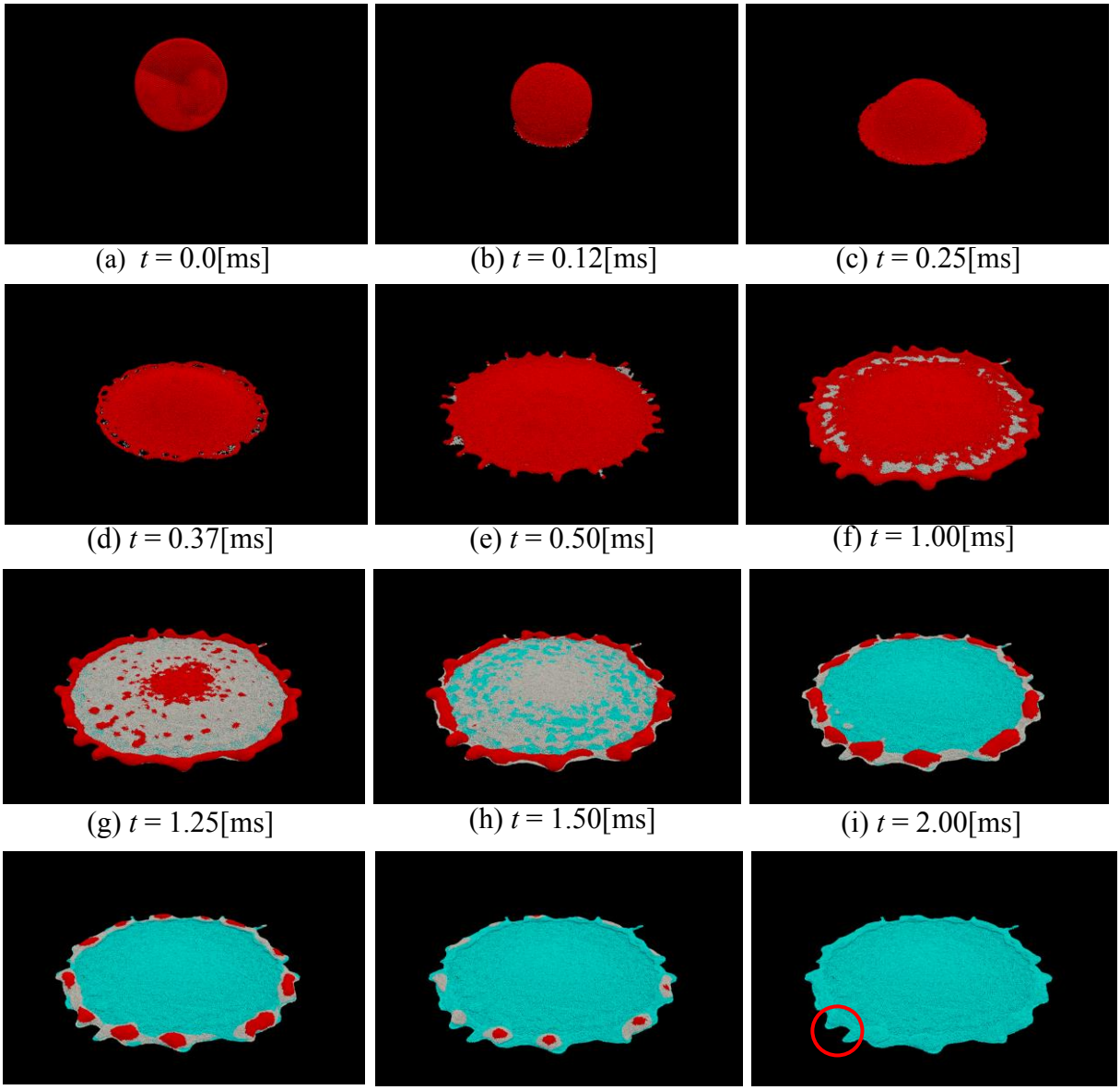

(a) t = 0.0[ms] (b) t = 0.12[ms] (c) t = 0.25[ms]

(d) t = 0.37[ms] (e) t = 0.50[ms] (f) t = 1.00[ms]

(g) t = 1.25[ms] (h) t = 1.50[ms] (i) t = 2.00[ms]

(j) t = 2.50[ms] (k) t = 3.50[ms] (l) t = 4.00[ms]

Figure 3 Time series of snapshots of the deposition of the Sn droplet in the case of the collision angle of 90 degree at the collision velocity of 4 m/s (bird's eye view).

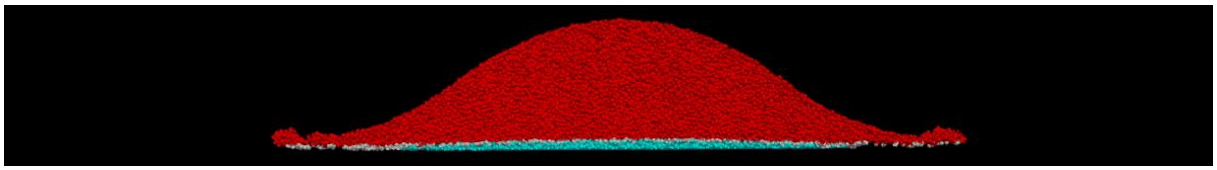

(a) t = 0.37[ms]

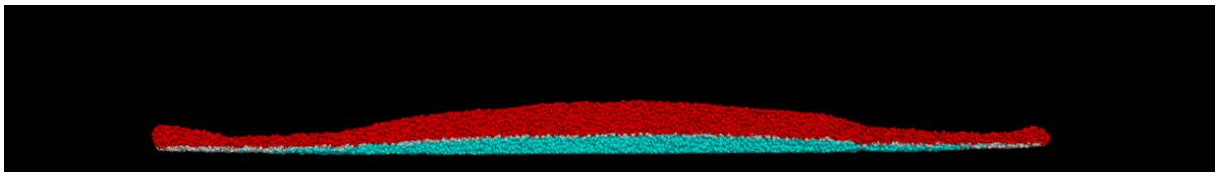

(b) t = 0.75[ms]

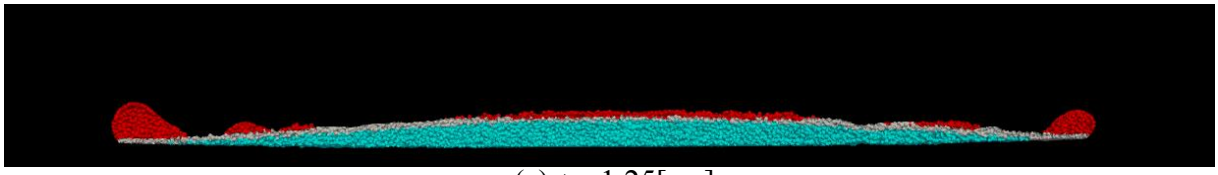

(c) t = 1.25[ms]

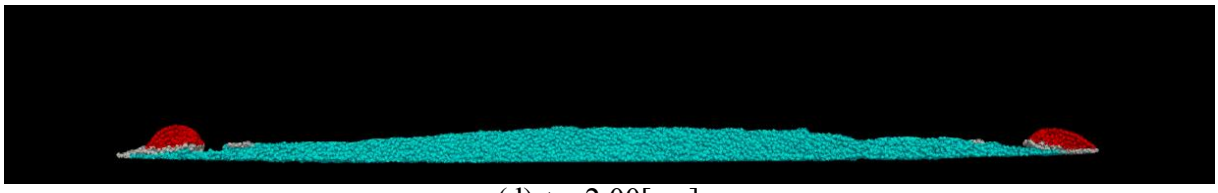

(d) t = 2.00[ms]

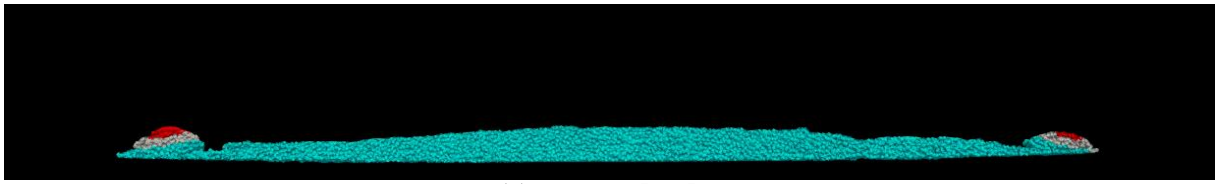

(e) t = 3.00[ms]

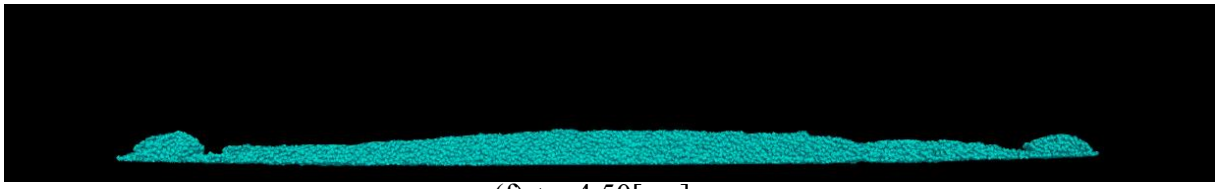

(f) t = 4.50[ms]

Figure 4 Time series of snapshots of the deposition of the Sn droplet in the case of the collision angle of 90 degree at the collision velocity of 4 m/s (side view).

Here, we evaluate a time variation of the droplet diameter spreading on the surface, quantitatively. Since the droplet has many fingers, there are some possible definitions of the diameter. Figure 5 describes the definition of the diameter D in the present study. We extract the finger which is closest to the x-axis and measure the x position of the top of the finger. The x-position is refereed to as the diameter of D. Although the strict maximum diameter of the droplet is the distance between the origin and the top of the nearest finger, the difference between D and the strict diameter is less than 2 % due to very small angle θ.

Figure 6 shows the time variation of the non-dimensional droplet diameter, D/D_0. D_0 is the initial diameter of the droplet, which is described in section 3. The dimensional time t begins when the droplet starts falling. At $t < 0.5$ [ms], the non-dimensional droplet diameter agrees with the experimental data [6]. In time advance, the non-dimensional diameter continues to increase at $t < 1.5$ [ms], then decreases slightly at 1.5 [ms] $< t < 2.5$ [ms], and reaches a steady state in both numerical and experimental results. The decrease of the diameter at 1.5 [ms] $< t < 2.5$ [ms] is due to the surface tension of the liquid phase of the droplet: the liquid runs off the finger, the surface tension suppresses to expand the diameter, and then the liquid comes back. Subsequently, the non-dimensional diameter reaches a steady state. We note that the resultant diameter is smaller than that of the experimental data [6]. Because the constant temperature is imposed as the boundary condition on the surface of the substrate in the present study, the solidification speed is faster and then the diameter in the transient and solid phase is smaller than the experimental results.

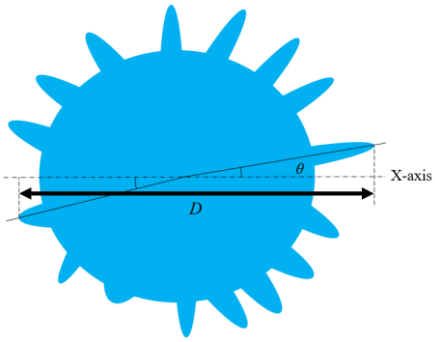

Figure 5 Definition of a diameter of an adhered droplet in the present study.

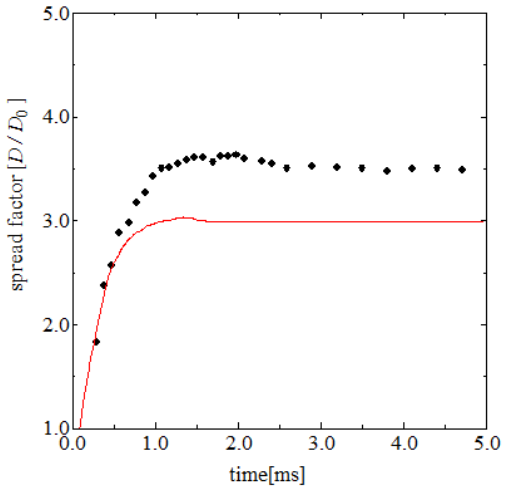

Figure 6 Time variation of non-dimensional droplet diameter: black line, the result in the present simulation at the collision velocity of 4 m/s; dot, the experimental data obtained by Shakeri et al. (2002) [6].

Figure 7 shows a times series of snapshots of coagulation behaviors of the Sn droplet in the cases of three different collision velocities, v_0 = 10, 20 and 30 [m/s]. The liquid, transient (i.e. liquid to solid), and solid particles are colored by red, white, and blue, respectively. As increase of the initial drop velocity, the number of splashing particles increases and finger-structures are not generated since many particles tend to rebound in the wall-normal direction.

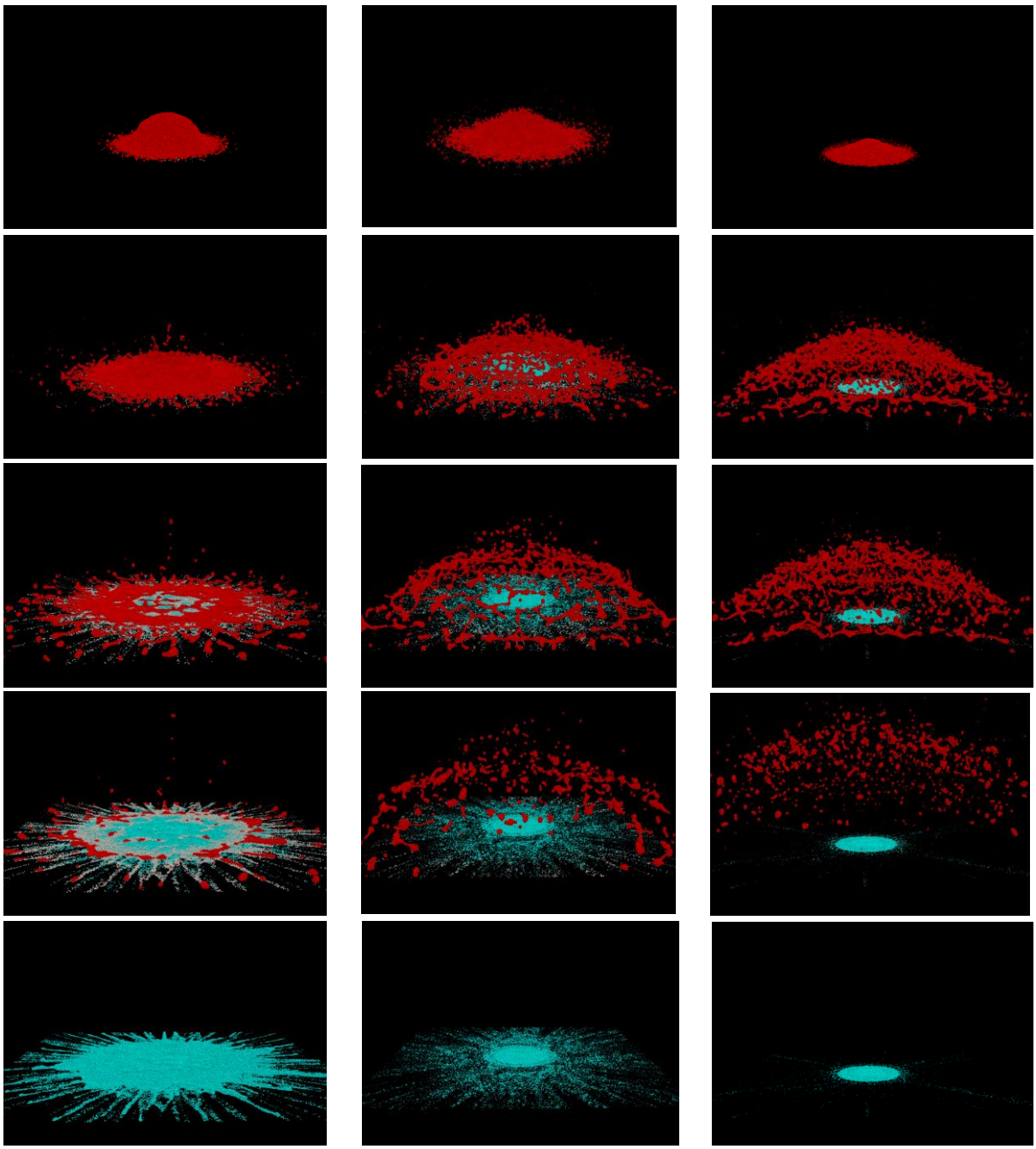

Figure 7 Time series of snapshots of deposition behavior of the Sn droplet for different initial velocities: left column, v_0=10 m/s; middle column, v_0=20 m/s; right column, v_0=30 m/s.

5 CONCLUSIONS

We perform numerical simulations on deposition phenomena of a single molten Sn droplet on a flat surface of the substrate in the cases of four different collision velocities by means of the E-MPS method. The latent heat is considered to reproduce the coagulation behaviors of the droplet. The results show that the simulation reproduces that the droplet collides, spreads, and coagulates on the substrate. The time variation of non-dimensional diameter obtained by the simulation shows the similar tendency to the existing experimental results. The quantitative difference between the numerical and experimental results is attributed to the difference of thermal boundary condition on the substrate surface. We also investigate effects of the impact velocity on behaviors of a colliding droplet. Finger-like-structures, which are a typical structure in the deposition, are observed at the circumference of the adhered droplet in cases of lower collision velocity, while finger-structures are not generated since many particles tend to rebound in cases of higher collision velocity.

REFERENCES

[1] S. Singh and D. K. Tafti, “Prediction of Sand Transport and Deposition in a Two-Pass Internal Cooling Duct”, ASME J. Engineer. Gas Turbines Power, 138, (2016), pp.1-12.

[2] J. Webb et al., “Coal Ash Deposition on Nozzle Guide Vanes - Part I: Experimental Characteristics of Four Coal Ash Types”, J. Turbomach., 135 (2013), 021033, pp.1-9.

[3] C. Josserand et al., “Drop Impact on a Solid Surface” Annu. Rev. Fluid Mech., 48 (2016), pp. 365-391.

[4] M. Oochi et al., “Explicit MPS Algorithm for Free Surface Flow Analysis”, Trans. Jpn. Soc. Comput. Eng. Sci., 20100013, (2010), 8 pp.

[5] R. Takahashi et al., “Development and Elaboration of Numerical Method for Simulating Gas-Liquid-Solid Three Phase Flows based on Particle Based Method.” Int. J. Comput. Fluid. Dyn., 30 (2016), pp. 120-128.

[6] S. Shakeri and S. Chandra, “Splashing of Molten Tin Droplets on a Rough Steel Surface”, Int. J. Heat Mass Transfer, 45, (2002), pp. 4561-4575.

[7] H. Ikeda, “Numerical Analysis of Fragmentation Processes in Vapor Explosions using Particle Method”, Doctoral Dissertation of the Tokyo University, (1999), pp. 63-69.

[8] H. Tabbara et al., “Modelling of Impingement Phenomena for Molten Metallic Droplets with Low to High Velocities”, Int. J. Heat Mass Transfer, 55 (2012), pp. 2081-2086.